JACS
JOURNAL OF THE AMERICAN CHEMICAL SOCIETY

Article

pubs.acs.org/JACS

Macrocyclized Extended Peptides: Inhibiting the Substrate-Recognition Domain of Tankyrase

Wenshu Xu,[†] Yu Heng Lau,[‡] Gerhard Fischer,[§] Yaw Sing Tan,[‡,∥] Anasuya Chattopadhyay,[†] Marc de la Roche,[§] Marko Hyvönen,[§] Chandra Verma,[∥,⊥,#] David R. Spring,*[,‡] and Laura S. Itzhaki*[,†]

[†]Department of Pharmacology, University of Cambridge, Tennis Court Road, Cambridge CB2 1PD, United Kingdom

[‡]Department of Chemistry, University of Cambridge, Lensfield Road, Cambridge CB2 1EW, United Kingdom

[§]Department of Biochemistry, University of Cambridge, 80 Tennis Court Road, Cambridge CB2 1GA, United Kingdom

[∥]Bioinformatics Institute, Agency for Science, Technology and Research (A*STAR), 30 Biopolis Street, #07-01 Matrix 138671, Singapore

[⊥]School of Biological Sciences, Nanyang Technological University, 60 Nanyang Drive 637551, Singapore

[#]Department of Biological Sciences, National University of Singapore, 14 Science Drive 4 117543, Singapore

Supporting Information

ABSTRACT: We report a double-click macrocyclization approach for the design of constrained peptide inhibitors having non-helical or extended conformations. Our targets are the tankyrase proteins (TNKS), poly(ADP-ribose) polymerases (PARP) that regulate Wnt signaling by targeting Axin for degradation. TNKS are deregulated in many different cancer types, and inhibition of TNKS therefore represents an attractive therapeutic strategy. However, clinical development of TNKS-specific PARP catalytic inhibitors is challenging due to off-target effects and cellular toxicity. We instead targeted the substrate-recognition domain of TNKS, as it is unique among PARP family members. We employed a two-component strategy, allowing peptide and linker to be separately engineered and then assembled in a combinatorial fashion via click chemistry. Using the consensus substrate-peptide sequence as a starting point, we optimized the length and rigidity of the linker and its position along the peptide. Optimization was further guided by high-resolution crystal structures of two of the macrocyclized peptides in complex with TNKS. This approach led to macrocyclized peptides with submicromolar affinities for TNKS and high proteolytic stability that are able to disrupt the interaction between TNKS and Axin substrate and to inhibit Wnt signaling in a dose-dependent manner. The peptides therefore represent a promising starting point for a new class of substrate-competitive inhibitors of TNKS with potential for suppressing Wnt signaling in cancer. Moreover, by demonstrating the application of the double-click macrocyclization approach to non-helical, extended, or irregularly structured peptides, we greatly extend its potential and scope, especially given the frequency with which such motifs mediate protein−protein interactions.

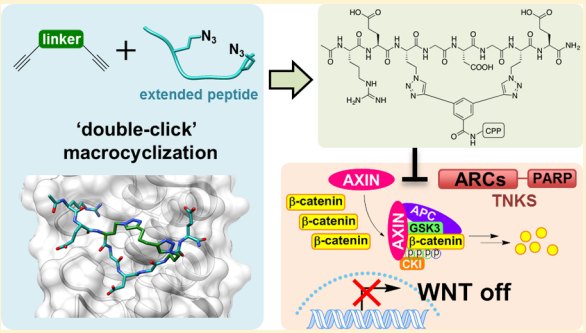

INTRODUCTION

The development of effective strategies for modulating protein−protein interactions (PPIs) has the potential to vastly expand the range of druggable proteins. Targeting the typically large, flat surfaces involved with molecules of high affinity and specificity can be readily achieved by mimicking the natural binding partner protein's interacting surface in the form of constrained peptides or peptidomimetics (reviewed in refs 1−5). The constraint serves the dual purpose of preorganizing the structure and thereby increasing the binding affinity as well as enhancing the pharmacokinetic properties such as in vivo stability and cell penetration.[6−9] Toward this goal, a class of molecules called "stapled" or constrained peptides have been developed, which are characterized by a bioactive, α-helical conformation that is induced by chemically cross-linking two side chains.[10−18] Constraining non-helical, extended, or irregularly structured peptide motifs presents a different challenge, as it is harder to rationally design a linker so as to stabilize a binding-competent conformation (e.g., ref 19). Given that these types of motifs are found in up to 50% of all PPIs,[20] there is a pressing need to address this challenge.

Here, we use a two-component double-click chemistry approach to macrocyclize peptides in an extended, non-helical conformation. Our targets are the tankyrase proteins. Tankyrase 1 and tankyrase 2 (subsequently referred to as TNKS) are poly(ADP-ribose) polymerases (PARPs) involved in a number of cellular processes. These include control of the mitotic checkpoint,[21−23] regulation of telomere length by targeting telomeric repeat binding factor 1 (TRF1) for degradation,[24−28]

Received: September 29, 2016
Published: January 13, 2017

DOI: 10.1021/jacs.6b10234
J. Am. Chem. Soc. 2017, 139, 2245−2256

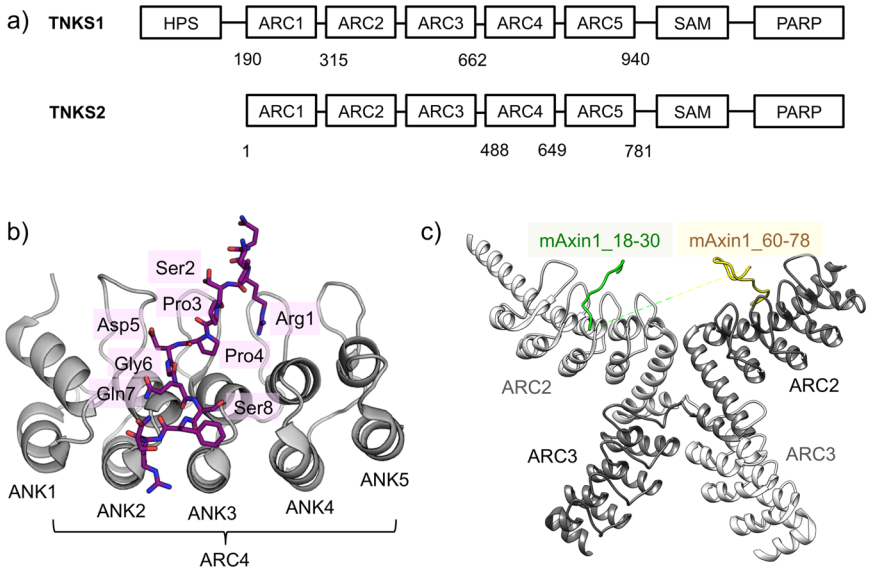

Figure 1. Structure of TNKS1 and TNKS2. (a) Domain architecture, comprising a homopolymeric run of histidine, proline and serine (HPS) residues, the ankyrin repeat cluster (ARC), sterile alpha motifs (SAM), and catalytic PARP domains. (b) Structure of human TNKS2 ARC4 (gray cartoon) in complex with substrate peptide LPHLQ**RSPPDGQS**FRS (purple; PDB ID: 3TWR);[53] for clarity, only the central part of the peptide (in bold) is labeled. (c) Structure of mouse TNKS1 ARC2−3 (gray cartoon) in complex with mouse Axin1_1−80; only residues 18−30 (green) and 60−78 (yellow) of mAxin1 are visible in the crystal structure (PDB ID: 3UTM).[54]

and regulation of Wnt signaling by targeting Axin for degradation.[29,30] Altered TNKS expression or activity is implicated in various disease states, and increased expression of TNKS has been observed in many different cancers including breast cancers, fibrosarcoma, ovarian cancer, glioblastoma, pancreatic adenocarcinoma, and gastric cancer.[28,31−34] As cancer therapeutics, TNKS inhibitors could potentially exploit tumor-specific Wnt dependency (e.g., in colorectal cancers with APC and KRAS mutations, which are resistant to epidermal growth factor receptor inhibitors) or target telomere dysfunction or an enhanced mitotic rate. It has also been shown that silencing of TNKS by RNAi has a synthetic lethality effect in tumor cells with BRCA1/BRCA2 gene defects but has minimal effects in wild-type cells.[32] Thus, TNKS inhibitors, like PARP inhibitors, may be useful for the treatment of breast cancers caused by mutations in the BRCA genes.[35−37] Furthermore, TNKS inhibitors may additionally have broader clinical applications. For example, the Wnt pathway has been found to be a valid target for treating neurodegenerative diseases (reviewed in refs 38 and 39), such as multiple sclerosis[40,41] and amyotrophic lateral sclerosis.[42,43] More recently, TNKS have been found to play a role in glucose homeostasis[44] in type II diabetes.

The first small-molecule TNKS inhibitor[29] (discovered in a Wnt pathway inhibitor screen) and those developed subsequently[45−48] are all directed against the catalytic PARP domain; however, there are problems of cellular toxicity due to off-target effects arising from the NAD+/ADP ribose-like characteristic of these active-site inhibitors (reviewed in refs 35 and 49−51). The TNKS proteins have a domain structure that is distinct from other PARP family members, as they contain an ankyrin domain comprising a series of ankyrin-repeat clusters (ARCs) that are involved in targeting specific proteins for PARylation (Figure 1a). Our aim herein was therefore to develop a new class of highly specific TNKS inhibitors by targeting the substrate-recognition domain. Moreover, Guettler et al. have recently shown that TNKS can induce Wnt signaling independently of its catalytic PARP activity, mediated instead via an ARC-domain scaffolding function and thus suggesting additional advantages of therapeutic targeting of this domain.[52]

To this end, we have designed a series of macrocyclized peptides using a modular two-component strategy that employs click chemistry to connect a linker and a peptide, thus allowing each to be varied independently before assembling them in a combinatorial fashion.[55,56] Our designs were guided by the previously determined crystal structures of substrate-derived peptides in complex with the fourth ARC domain of TNKS2 (TNKS2 ARC4) (Figure 1b)[53] and subsequently optimized with the help of molecular dynamics (MD) simulations using an iterative process of modifying the length and rigidity of the linker as well as its position along the peptide sequence. We determined the crystal structures of two of the macrocyclized peptides in complex with TNKS, leading to further optimization of the design. We show that these peptides are able to disrupt tankyrase-substrate complexes in vitro and to inhibit Wnt transcription in a dose-dependent manner. Thus, our results provide a promising starting point for a new class of substrate-competitive inhibitors of tankyrase. Moreover, the methodology has the potential to be a general approach for inhibiting PPIs that involve non-helical, extended, or irregularly structured molecular recognition motifs.

RESULTS

Peptide and Linker Design. We focused the design and optimization strategy on an 8-residue consensus sequence, REAGDGEE, derived previously from a mutational analysis of TNKS substrates.[53] In that study, a 10-residue peptide was found to be sufficient for high-affinity TNKS binding; we demonstrate here that further truncation to the 8-core binding residues does not weaken the affinity of the peptide. Computational alanine scanning was first carried out on structures extracted from three independent 50 ns MD simulations of the complex between TNKS2 ARC4 and the 8-residue consensus sequence (for which there are no available

DOI: 10.1021/jacs.6b10234
J. Am. Chem. Soc. 2017, 139, 2245−2256

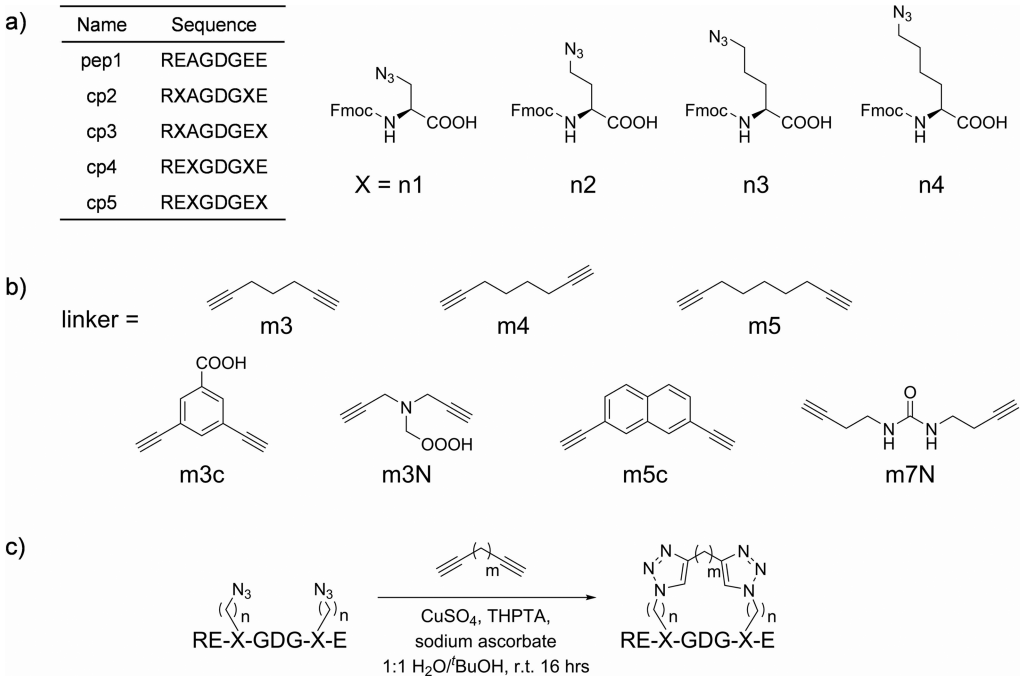

Figure 2. Macrocyclic peptide design. (a, left) Sequences of the synthesized peptides with the UAAs denoted as 'X'; (right) chemical structures of the different UAA side chains, where n2, n3, and so forth indicate the number of CH_2 units in the side chain. (b) Chemical structures of the linkers, where m3–m5 indicate the number of carbon/nitrogen atoms between the two alkynyl groups. (c) Schematic of the click reaction between the peptides in (a) and linkers in (b); see Figure S2 for full chemical structures of representative peptides.

experimental structures) to assess which positions would be amenable to replacement by an unnatural amino acid (UAA) having azido functionality for conjugation to the linker. The analysis indicated Arg1 to be an important hot-spot residue, whereas Ala3 (mutated to Gly in the computational analysis), Asp5, and Glu8 make only modest contributions to the interaction (Figure S1). The modeling also suggests that positions 4 and 6 are unfavorable for cross-linking due to a high likelihood of steric clashes of their side chains with the protein surface. Mutations of Glu2 and Glu7 were found to be stabilizing, indicating that the wild-type residues are detrimental to binding and consequently amenable to replacement by UAAs. Thus, a first panel of macrocyclized peptides was synthesized with azido-functionalized UAAs at positions 2 or 3 and 7 or 8 (Figure 2a), and they were acetylated at the N-terminus to neutralize the terminal charge. The UAA side chains are denoted n1–n4 to indicate the number of methylene (CH_2) units (Figure 2a).

We explored a number of different linker designs, varying both the chemical properties and rigidity (Figure 2b). All linkers contained an alkyne at each terminus to cross-link the two UAAs in the peptide. Linkers with linear aliphatic units between the two alkynyl groups are denoted m3–m5 to indicate the number of methylene (CH_2) units. These linkers were commercially available. A longer linker containing hydrocarbon units and a urea derivative, which we denote as m7N, was synthesized from 1,1′-carbonyldiimidazole and 1-amino-3-butyne (protocols modified from ref 57). The linkers with greater rigidity, m3c and m5c, contain aromatic groups and were synthesized using palladium-catalyzed coupling chemistry.[56,58]

The Double-Click Reaction Can Effectively Macrocyclize Extended Peptides. We previously used our double-click chemistry strategy to staple α-helical peptides derived from the tumor suppressor p53 for inhibition of the p53-Mdm2 interaction.[56] In that case, as for other helix stapling methods, the stapling positions were identified to be the *i*, *i*+4 or *i*, *i*+7 residue pairs so that the intrinsic helical propensity of the peptide brings the two stapling positions close together in space, thereby helping to drive the reaction.[6−8] The TNKS-bound peptides adopt an extended conformation, and therefore, we first tested the efficiency of the click reaction between linker and peptide in this context. After optimization of the reaction conditions, we were able to show that the click reaction between peptide cp4n4 and linker m5 proceeded to completion after stirring overnight under nitrogen in degassed solvent (Figure 2c). Monitoring by liquid chromatography mass spectrometry (LCMS) showed that no starting material remained and that there was a single product with the expected mass. The purified and lyophilized product was further analyzed by infrared spectrometry (IR) and high-resolution mass spectrometry to verify that the two azido groups in the peptide reacted with the same linker because other potential byproducts share the same mass from the 1,3-dipolar cycloaddition. The disappearance of the typical azido stretch at 2100 cm^{-1} in the IR spectrum after the reaction suggested that both azido groups had reacted (Figure S4). The isotopic patterns from mass spectrometry showed a mass spacing between two $[M + 2H]^{2+}$ species of 0.5 amu, consistent with the cross-linking of a single linker onto one peptide (Figure S5). These results demonstrate unequivocally that we can extend the scope of our two-component click macrocyclization strategy to non-helical peptides.

The affinities of a first panel of macrocyclized peptides for binding to TNKS2 ARC4 were determined using a competitive fluorescence polarization (FP) assay with a TAMRA-labeled linear peptide T-pep1 (TAMRA-Ahx-REAGDGEE, where Ahx is a spacer that comprises 6-aminohexanoic acid; TAMRA-

DOI: 10.1021/jacs.6b10234
J. Am. Chem. Soc. 2017, 139, 2245−2256

labeled peptides are indicated with "T-" at the beginning of the name) as the competing ligand (Figure 3 and Table S1). The

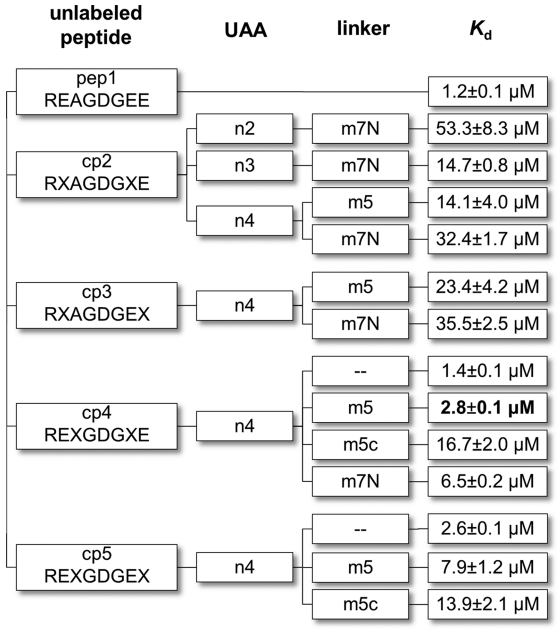

Figure 3. Determining the optimal peptide-linker combination. Dissociation constants were determined by competitive FP assay using labeled T-pep1 bound to ARC4 as the tracer for the first panel of macrocyclized peptides in which we varied the positions of the two UAAs (denoted X) in the peptide sequence, the lengths of the side chains, and the length of the linker. "*n*" is the number of methylene (CH_2) groups in the side chain of the UAAs; '*m*' is the number of carbon/nitrogen atoms between the two triazole groups in the linker. Special linkers are m5c, a rigid linker based on napthalene, and m7N, a linear linker made from a urea derivative described earlier. A dash in the "*m*" box denotes uncross-linked peptide. The dissociation constant of the unlabeled linear peptide, pep1, is shown for comparison. Uncross-linked cp4n4 and cp5n4 were measured as comparisons to their cross-linked counterpart. A full list of dissociation constants is given in Table S1.

dissociation constant of the labeled T-pep1 was 0.8 ± 0.1 μM from the direct FP measurement, and that of unlabeled pep1 was 1.2 ± 0.1 μM from the competitive FP measurement in agreement with the values reported in the literature.[53] Two uncross-linked precursor peptides, cp4n4 and cp5n4, were also tested and found to have affinities that were similar to or only slightly weaker than pep1, indicating that incorporation of the UAAs did not significantly perturb the interaction with TNKS ARC4. All of the macrocyclized peptides in this first panel bound more weakly than the linear pep1 to TNKS ARC4. We tested several combinations of UAAs and linkers based on cross-linking positions 2 and 7 (RXAGDGXE; cp2), including varying the UAA side chain lengths (*n*) between 2 and 4, and two different linker lengths (*m*) of 5 and 7; however, all combinations yielded peptides that exhibited very weak binding affinities. Macrocyclization of cp3, containing UAAs in positions 2 and 8, also yielded weak binding affinities. Macrocyclization of cp4 and cp5 (UAAs in positions 3 and 7/8), however, yielded higher binding affinities, and peptide REXGDGXE (cp4) was therefore chosen for further optimization.

Crystal Structures of TNKS2 in Complex with the Macrocyclized Peptides. To aid the design process, we determined the structure of cp4n4m5 (Figure S2) in complex with TNKS2 ARC4 (Figure 4 and Figures S6 and S7). This structure shows that the binding mode of the macrocyclized peptide is very similar to that of the natural peptides. Specifically, Arg1 of cp4n4m5 forms two salt bridges with Glu598 and Asp589 of TNKS2 ARC4 (Figure S6a) and Glu2 with TNKS2 Lys557 (Figure S6b). The side chains of the two UAAs, UAA3 and UAA7, point away from the protein surface, which is crucial for their ability to form a macrocycle that does not interfere with protein binding (Figure 4b). Between UAA3 and UAA7, residues Gly4, Asp5, and Gly6 of the peptide fit inside a groove on the protein surface (Figure 4a and Figure S6c) with hydrogen bonding between Asp5 and TNKS2 Ser527 (Figure S6d) and the phenol rings of Tyr569 and Tyr536 stacking in parallel on either side of Gly6 (Figure S6c). The C-terminal residue of cp4n4m5, Glu8, interacts with TNKS2 Lys604 via a salt bridge (Figure S6e). We note that the linker is positioned away from the binding surface and does not perturb the interactions between cp4n4m5 and TNKS2 ARC4 (Figure 4b), and it should therefore be possible to install additional functionalities on the linker without compromising the binding interface. Despite the high 1.35 Å resolution of the crystal structure, parts of the UAA side chains and the triazole-containing linkage are poorly defined in the election density (Figure 4b). This suggests that shortening the UAA side chains and the linker should lead to tighter binding by further reducing conformational flexibility.

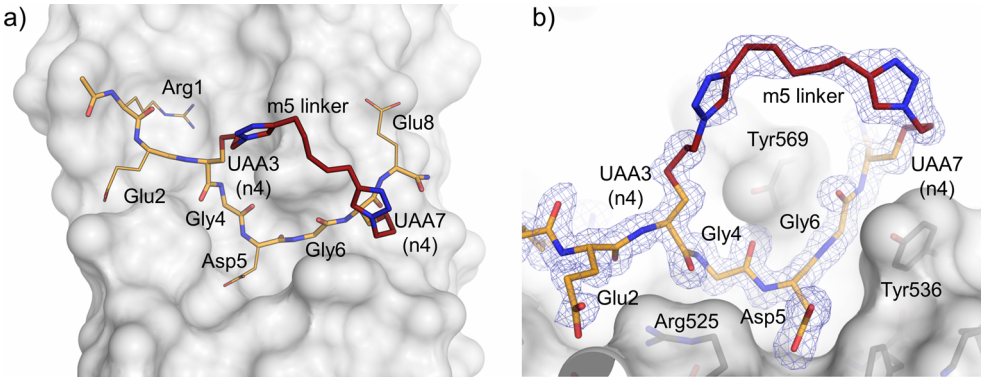

Figure 4. (a) Crystal structure of TNKS2 ARC4 (gray surface) in complex with the macrocyclized peptide cp4n4m5 (orange carbons; linker in red). (b) $2F_{obs} - F_{calc}$ electron density (blue mesh) of the linker and of the central residues of the peptide (orange; linker in red) contoured at 1σ, rotated approximately 90° along the horizontal axis compared to (a).

DOI: 10.1021/jacs.6b10234
J. Am. Chem. Soc. 2017, 139, 2245−2256

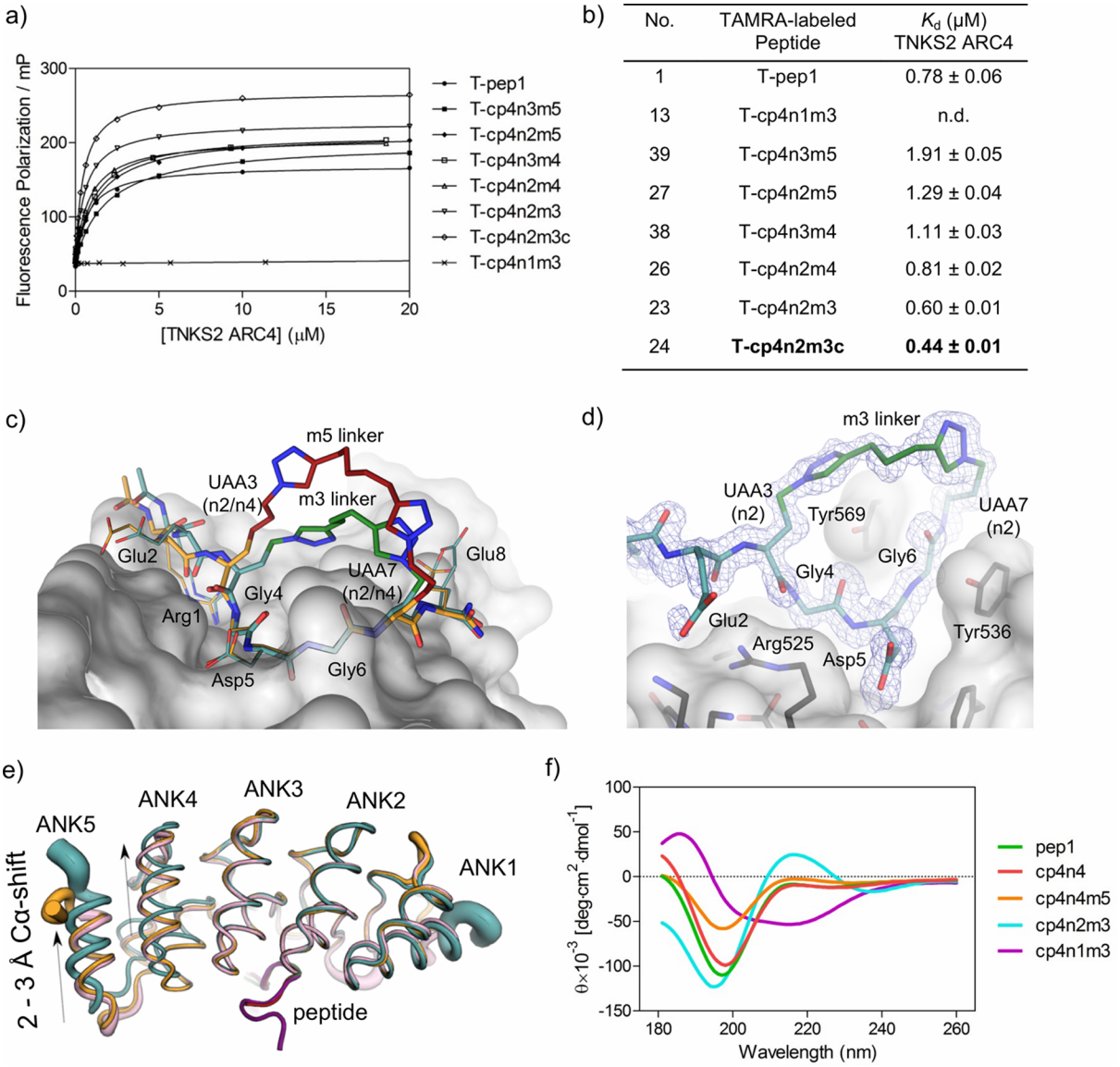

No.	TAMRA-labeled Peptide	K_d (μM) TNKS2 ARC4
1	T-pep1	0.78 ± 0.06
13	T-cp4n1m3	n.d.
39	T-cp4n3m5	1.91 ± 0.05
27	T-cp4n2m5	1.29 ± 0.04
38	T-cp4n3m4	1.11 ± 0.03
26	T-cp4n2m4	0.81 ± 0.02
23	T-cp4n2m3	0.60 ± 0.01
24	**T-cp4n2m3c**	**0.44 ± 0.01**

Figure 5. (a) Direct FP measurements for a subset of the second panel of TAMRA-labeled peptides based on the cp4 sequence (TAMRA-Ahx-REXDGDXE) with (b) their binding affinities listed in a table (see Table S2 for the full list of peptides and their binding affinities). The K_d for T-cp4n1m3 is not detectable (n.d.). (c) Crystal structure of TNKS2 ARC4 (gray surface) in complex with macrocyclized peptide cp4n2m3 (cyan; linker in green). Superposition of cp4n2m3 (cyan/green) and cp4n4m5 (orange/red) in the two structures of the complexed peptides; TNKS2 ARC4 is shown in gray. (d) $2F_{obs} - F_{calc}$ electron density, contoured at 1σ, of the linker and of the central residues of peptide cp4n2m3. (e) Overlay of the three structures: the complex with the natural substrate peptide LPHLQRSPPDGQSFRS is shown (PDB ID: 3TWR)[53] (protein: pink; peptide: purple). Ankyrin repeats 4 and 5 of TNKS2 ARC4-cp4n2m3 (cyan) move by 2−3 Å compared to those in the complex with cp4n4m5 (orange) and the linear peptide (pink). (f) CD spectra of linear peptides pep1 (green) and cp4n4 (red) and of cross-linked peptides cp4n4m5 (orange), cp4n2m3 (cyan), and the non-binding cross-linked peptide cp4n1m3 (purple).

Consequently, we next synthesized UAAs with shorter side chains and incorporated them into the cp4 sequence. All of the peptides were synthesized with a TAMRA label at the N-terminus (TAMRA-Ahx-REXGDGXE) for use in the direct FP assay format. The number (n) of CH_2 groups in the side chain of each UAA was varied between 1 and 3, and the number of carbon/nitrogen atoms (m) between the two triazole groups in the linker was varied between 3 and 5 (Figure 5a and b and Table S2). We found that the binding affinity was always weakened when non-identical UAAs were used in the same peptide, and it was greatly weakened with UAA side chain length of n = 1. Upon shortening of the linker, the binding affinity progressively increased, and rigidifying the linker by incorporating an aromatic moiety (linker m3c) resulted in a further increase of the affinity. The macrocyclized peptide with the highest binding affinity had n = 2 for both UAA side chains and the rigid linker m3c (labeled T-cp4n2m3c, Figures S2 and S3); its affinity is approximately 2-fold higher than that of the linear peptide T-pep1.

We then synthesized the unlabeled version of the highest affinity peptides from this second round of design and determined the structure of TNKS2 ARC4 in complex with one of them, cp4n2m3 (Figure 5, and Figures S2, S3, and S7a). When comparing this structure with that of TNKS2 ARC4-cp4n4m5 and those of previously published natural peptides,[53] we can see that the linkers of both cp4n4m5 and cp4n2m3 are long enough to retain the binding mode of the natural peptide (Figure S7b). Additionally, the TNKS2 protein itself appears to

DOI: 10.1021/jacs.6b10234
J. Am. Chem. Soc. 2017, 139, 2245−2256

have some flexibility for accommodating the slightly different conformations of the peptides.

Both peptides are more flexible at their respective termini (see Figures S7 and S8), whereas the central regions make close contacts with TNKS2 ARC4 and adopt virtually identical conformations in the two macrocyclized peptides (Figure 5c). The central residues Gly4-Asp5-Gly6 are deeply inserted into a binding cleft of the protein, forming several hydrogen bonding interactions as well as remarkable π-stacking interaction, wherein Gly6 is sandwiched between Tyr536 and Tyr569 (Figures 4b and 5d and Figure S7c). Shortening of the UAA side chains and the hydrocarbon linker rigidifies the macrocycle, which is corroborated by the better-defined electron density of cp4n2m3 (Figure 5d and Figure S7d). The shorter linker of cp4n2m3 pulls the side chains of peptide residues 3 and 7 slightly inward when compared with that of the wild-type peptide (PDB ID: 3TWR)[53] and cp4n4m5 (Figure 5c and Figure S7b).

This difference appears to have an effect on the overall protein curvature, whereby ankyrin repeats 4 and 5 move by 2−3 Å (Figure 5e). Although we cannot exclude a crystallization artifact caused by changes in the packing of the complexes in the two different crystal forms (Table S3), we could not observe a change of this type in any of the previously published linear peptide complexes (PDB IDs: 3TWR, 3TWS, 3TWT, 3TWU, 3TWV, 3TWW, and 3TWX),[53] and the resolution of 1.33 Å should be sufficient to reliably observe these differences. This alternative conformation was very similar to the crystal structure of the apo protein (PDB ID: 3TWQ; Figure S9a) with the only discernible difference found in ankyrin repeat 5. Accordingly, this change in protein conformation mainly affects the C-terminal end of the bound peptide: whereas Glu8 of cp4n4m5 forms a salt bridge with Lys604 (Figure S6e), in cp4n2m3, it instead forms an interaction with Lys602 (Figure S6f). Observed intermittently in MD simulations of the TNKS2 ARC4-pep1 complex (Figure S9b), this "apo-like" bound conformation allows for the formation of a novel water network that connects Glu8 and Lys602 with the triazole moiety of UAA3 in the TNKS2 ARC4-cp4n2m3 complex. An MD simulation of the isolated TNKS2 ARC4 sampled mainly the apo-like bound conformation (Figure S9c). Conformations that are somewhat similar to those observed in the linear peptide and cp4n4m5 complexes, except for slight differences in ankyrin repeats 3 and 5, were also sampled (Figure S9c). The fact that the unbound protein is able to adopt the apo-like bound conformation prior to binding suggests that conformational selection plays a dominant role in the binding of cp4n2m3, whereas the requirement for modest conformational changes in two of the ankyrin repeats suggests that induced fit mechanism is likely to be prominent in the binding of the linear peptides and cp4n4m5.

To better understand the effect of the different macrocycles on the conformations of the peptides and how any differences might translate into the order of binding abilities observed, we performed circular dichroism (CD) on the unlabeled peptides (Figure 5f). We find that linear pep1 and uncross-linked cp4n4 exhibit a random-coil conformation, as does the macrocyclic cp4n4m5. For the higher-affinity binder cp4n2m3, although its CD spectrum resembles that of a random coil with a minimum at 196 nm, it also has a small positive maximum at 217−218 nm similar to that of a collagen;[59] this distinctive secondary structure is presumably due to the tighter constraint restricting the flexibility of the peptide backbone. It is consistent with our goal of designing the macrocycles to restrict the conformations of the peptides to reduce the entropy cost of binding as further evidenced in the isothermal titration calorimetry data shown below. When we further reduce the length of the macrocycle in cp4n1m3, a macrocyclic peptide with nondetectable K_d for TNKS2 ARC4 (Figure 5a and b and Table S2), the CD spectrum indicates that an α-helical structure is induced by the tighter constraint. Analysis of the crystal structures also shows clearly that shorter UAAs (n = 1) would constrain the macrocycle too much for the peptide to form ideal interactions with the protein, leading to the observed weaker binding for n = 1 peptides (Table S2).

Macrocyclized Peptides Are Resistant to Proteolytic Degradation. For the effects of macrocyclization on peptide stability to be tested, representatives of both the linear and the macrocyclized peptides were subjected to proteolytic degradation using the AspN protease, which cleaves the N-terminal to aspartates, in this case, Asp5, which is located within the macrocycle. Protection of the central residues, Gly4-Asp5-Gly6, is crucial for the integrity of the peptide for fitting inside the binding groove of the protein. TAMRA-labeled peptides were used for monitoring the degradation based on the TAMRA signal at 550 nm wavelength. The majority of the linear peptide, T-pep1, was degraded within 1 h at room temperature, whereas nearly 100% of the macrocyclized peptide, T-cp4n2m3, remained intact after 4.5 h of peptidase treatment (Figure S10a). No mass corresponding to the possible degraded products could be found in the sample of the treated T-cp4n2m3 after 4.5 h (Figure S10b). These results show that macrocyclization greatly enhances the stability of the peptide.

Thermodynamics of the TNKS−Peptide Interactions. Isothermal titration calorimetry (ITC) was used to characterize the thermodynamics of the TNKS−peptide interactions (Figure 6, Figure S11, and Tables S4 and S5). The smaller $-T\Delta S$ terms obtained for the macrocyclized peptides compared with linear peptide pep1 are consistent with the goal of macrocyclization, which is to lock the peptide in an active conformation and thereby minimize the entropic cost of binding (Figure 6). Furthermore, a smaller $-T\Delta S$ value was

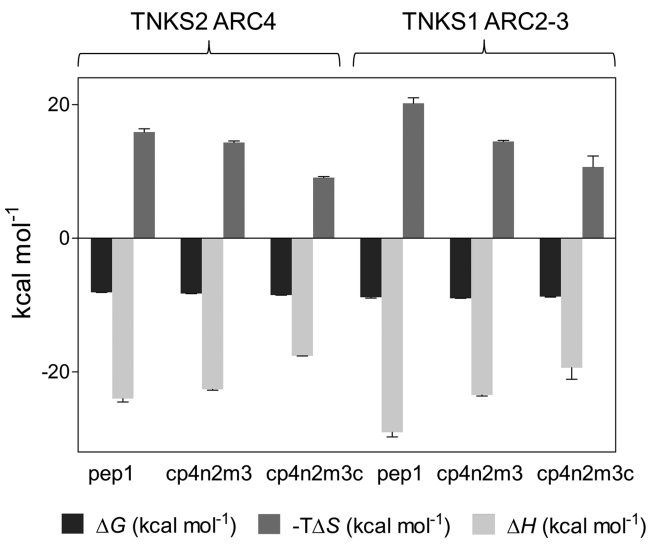

Figure 6. Thermodynamic parameters obtained for the binding of the peptides to TNKS2 ARC4 and to TNKS1 ARC2−3, as measured by ITC. Error bars are those obtained from standard derivation of the mean from duplicate measurements.

DOI: 10.1021/jacs.6b10234
J. Am. Chem. Soc. 2017, 139, 2245−2256

obtained for peptide cp4n2m3c with the more rigid linker compared with that of cp4n2m3, consistent with the success of this design feature.

TNKS proteins contain five ARCs, of which ARC2, 4, and 5 have sites for recognition by TNKS binding motifs. We therefore also tested the binding of the peptides to TNKS1 ARC2−3, a construct containing ARC2 and (non-binding) ARC3, whose structure had previously been solved.[54] We obtained similar results to TNKS2 ARC4 in terms of the relative ΔS values of pep1 and the two macrocyclized peptides. We note that all of the peptides tested bound more tightly to TNKS1 ARC2−3 than to TNKS2 ARC4 (Tables S4 and S5), although the two ARC domains share almost identical residues at the binding interfaces.

We next compared the thermodynamic parameters of the peptides with those of the TNKS substrate Axin. Axin is a rate-limiting component of the β-catenin destruction complex in the Wnt sigaling pathway, and PARylation of Axin by TNKS leads to Axin degradation by the proteasome. The crystal structure of mouse TNKS1 ARC2−3 had previously suggested that dimerization of ARC2−3 occurs upon interaction with a fragment (residues 1−80) of mouse Axin1[54] because this fragment contains not one but two TNKS binding motifs, both of which are similar in sequence to the consensus sequence deduced by Guettler et al.[53] (Figure 1c). The two motifs of Axin (residues 18−30 and 60−79) each interact with one ARC2 subunit in the ARC2−3 dimer. We performed ITC using fragments of human Axin1, which share high homology to the mouse counterparts. Our ITC data are consistent with the dimerization of TNKS1 ARC2−3 seen in the crystal structure in that we also observe a stoichiometry of two TNKS1 ARC2−3 molecules binding to one Axin1_1−80 molecule (Table S5); a stoichiometry of 1 was obtained for the interaction of TNKS2 ARC4 with Axin1_1−80. Furthermore, the TNKS2 ARC4 binding affinity of Axin1_1−43 (containing only the N-terminal TNKS-binding motif) was similar to that of Axin1_1−80 (containing both motifs) (Table S4), indicating that the N-terminal motif is the main contributor to the TNKS2 ARC4 interaction, as was found to be the case for the TNKS1 ARC2−3 interaction.[54] Lastly, the ITC data show that both cp4n2m3 and cp4n2m3c are better binders than Axin1 to TNKS1 ARC2−3 as well as to TNKS2 ARC4, a result that was also confirmed by fluorescence polarization (Tables S4 and S5).

The Macrocyclized Peptides Disrupt the TNKS−Axin Interaction. Next, we tested the ability of the peptides to disrupt the TNKS−Axin interaction using an in vitro pull-down assay with TNKS2 ARC4 and GST-tagged human Axin1_1−80 immobilized on glutathione beads (Figure 7). The immobilized TNKS2 ARC4-Axin1_1−80 complex was incubated with increasing concentrations of linear peptide pep1 or macrocyclized peptide cp4n2m3 for 0.5 h. After washing the resin, the proteins remaining bound to the resin were analyzed by SDS-PAGE. The results show that pull-down of TNKS2 ARC4 was disrupted by the peptides in a dose-dependent manner. Macrocyclized peptide cp4n2m3 was a slightly better inhibitor than pep1 (IC_{50} of ~20 and ~40 μM, respectively), reflecting its slightly higher TNKS binding affinity.

Incorporation of Cell-Penetrating Capability into the Peptide Linker. We attached one of four different cell-penetrating peptide (CPP) sequences onto cp4n2m3c via the linker by synthesizing the CPP sequences with the m3c linker conjugated to their N-termini (see schematic in Table S6). The two-component double-click reaction was then performed

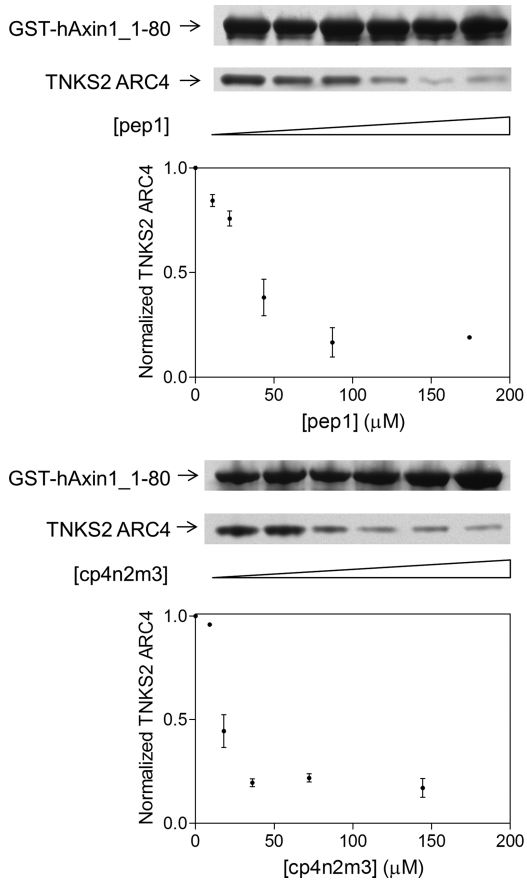

Figure 7. Competition of peptides with GST-tagged human Axin1_1−80 for binding to TNKS2 ARC4. The TNKS2 ARC4-Axin1_1−80 complex, immobilized on glutathione beads, was incubated with increasing concentrations of peptide. After washing, the protein remaining bound to the resin was run on SDS-PAGE. The TNKS2 ARC4 band was quantified using densitometry and normalized against the GST-Axin1_1−80 band. The data are plotted relative to the sample without peptide incubation (which was set at a value of 1).

between the CPP-conjugated m3c linker and the peptide T-cp4n2 (TAMRA-Ahx-REXGDGXE, where X is n2). In the case of the penetratin peptide (a 16-residue cell-penetrating sequence from the Antennapedia homeodomain[60]), we found that we needed two Ahx spacers between the CPP and the m3c linker for the click reaction to reach completion, as this relatively long cell-penetrating sequence appeared to otherwise inhibit the click reaction presumably for steric reasons. Next, we checked the TNKS2 ARC4 binding affinities of the TAMRA-labeled CPP-conjugated peptides using direct FP (Table S7). For the Arg_9 cell-penetrating sequence, when we used the two Ahx spacers we observed a degree of non-specific binding to TNKS2 ARC4, likely due to the arginine residues attached via the long flexible spacers competing with the binding peptide for a hotspot interaction on the protein, and therefore, this conjugate was not used further. We did not observe any non-specific binding for the other CPP-conjugated peptides shown in Table S7. All four exhibited TNKS binding affinities that are similar to that of the unconjugated counterpart T-cp4n2m3c. We next tested the cell-penetrating capabilities of the TAMRA-labeled peptides using U2OS and HEK 293T cells. Three of the CPP-conjugated macrocyclized peptides, T-cp4n2m3c-R_6, T-cp4n2m3c-R_9, and T-cp4n2m3c-Antp, showed significant fluorescence spreading across the whole cell even at the lowest

DOI: 10.1021/jacs.6b10234
J. Am. Chem. Soc. 2017, 139, 2245−2256

concentration of 10 μM. In contrast, T-cp4n2m3c-LCLR (LCLR is a cell-penetrating tetrapeptide derived from the X-protein of the hepatitis B virus[61,62]) and the non-conjugated peptides T-cp4n2m3 and T-cp4n2m3c exhibited only punctate fluorescence indicative of endosomal entrapment, and the linear peptide T-pep1 showed very weak fluorescence or no fluorescence at all (Figure S12).

The Macrocyclized Peptides inhibit Wnt Signaling. A dual-luciferase reporter (DLR) assay in Wnt-activated HEK 293T cells was used to determine the ability of the peptides to modulate β-catenin levels and suppress Wnt transcription. Unlabeled CPP-conjugates, rather than the TAMRA-labeled versions, were used in the experiments because rhodamine-based fluorescent labels have been found to cause cytotoxicity once they are transported intracellularly with the aid of CPP peptides.[63] Treatment of HEK 293T cells with an increasing concentration of unlabeled peptide cp4n2m3c-Antp (containing the penetratin sequence on the linker) led to a dose-dependent decrease in Wnt pathway reporter activity with an IC_{50} around 50 μM (Figure 8). There was no observed change

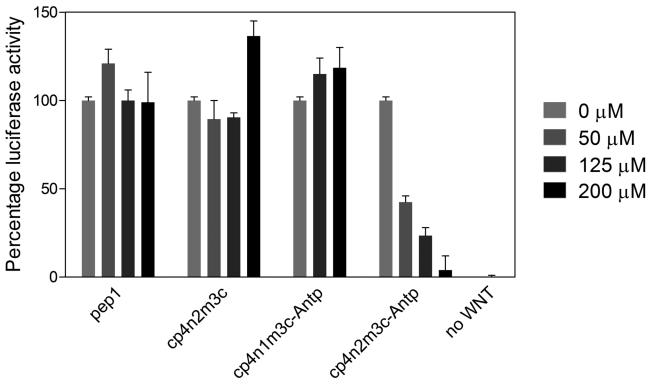

Figure 8. Effect on Wnt-activated HEK 293T cells of treatment with representative peptides. Error bars are those obtained from triplicate sample measurements from two independent experiments.

in the level of the control Renilla luciferase activity, indicating that peptide treatment had no effect on transcription in general. Moreover, treatment with non-cell-penetrating peptides pep1 or cp4n2m3c had no effect on Wnt reporter activity, nor did treatment with cp4n1m3c-Antp (a cell-penetrating version of the non-binding peptide cp4n1m3c) (Table S2), thereby satisfying these specificity controls. Figure S13 shows that none of the unlabeled peptides were cytotoxic at the concentrations used in the Wnt signaling assays.

SUMMARY

Here, we employed molecular dynamics simulations, two-component double-click macrocyclization, and combinatorial use of different non-natural amino acids and cross-linkers to constrain peptides that have extended bioactive conformations. We demonstrate the application of this approach to design inhibitors of the substrate-recognition domain of the TNKS proteins whose activity is deregulated in numerous cancers. One advantage of the two-component strategy is that the peptide and the linker can be engineered separately and then used in a combinatorial fashion to efficiently generate an array of molecules. With the consensus-optimized substrate sequence as a starting point, we used an iterative process of macrocyclized peptide design in which we varied the length and rigidity of the linker as well as its position along the peptide. The design was further guided by determining the crystal structures of two of the macrocyclized peptides in complex with TNKS. In this way, we identified peptides with submicromolar TNKS binding affinities that are proteolytically stable and capable of disrupting the interaction between TNKS and the Axin substrate in a dose-dependent manner. We exploited the two-component nature of the macrocyclization method to introduce cell-penetrating capability via the linker, and we showed that these peptides are indeed able to enter cells and modulate β-catenin levels. Thus, these macrocylized peptides represent a promising new class of substrate-competitive inhibitors of TNKS with potential for suppressing Wnt signaling in cancer. Moreover, we have demonstrated that double-click macrocyclization can be applied to non-helical, extended, or irregularly structured peptide conformations; we have also recently used it to develop constrained peptide inhibitors of the hepatocyte nuclear factor 1β transcription factor (HNF1β)−Importin α interaction in ovarian clear cell carcinoma.[64] Thus, the double-click macrocyclization strategy has a broad scope, especially given the frequency with which non-helical motifs are found in mediating PPIs.

EXPERIMENTAL SECTION

Molecular Dynamics Simulations. The structure of human TNKS2 ARC4 bound to a 3BP2-derived peptide (PDB ID: 3TWR[53]) was used to model the complex of TNKS2 ARC4 and the consensus tankyrase-binding peptide. The 3BP2-derived peptide was truncated to the core binding 8-residue motif (RSPPDGQS) and then modified into the consensus peptide (REAGDGEE) by using the tleap module of AMBER 11 to change the side chains of the mutated residues. The consensus peptide was capped by acetyl and amide groups. Protonation states of the complex were determined by PDB2PQR.[65] The LEaP program in AMBER 11 was then used to solvate the complex with TIP3P[66] water molecules in a truncated octahedral box, such that its walls were at least 9 Å away from any atom of the protein or peptide, followed by neutralization of the system with seven sodium ions.

Three independent explicit-solvent MD simulations of the modeled tankyrase complex were carried out using different initial atomic velocities. A separate MD simulation of the unbound TNKS2 ARC4 was also carried out. Energy minimizations and MD simulations were performed using the ff99SB-ILDN[67] force field with the sander and PMEMD modules of AMBER 11,[68] respectively. SHAKE[69] was applied to constrain all bonds involving hydrogen atoms, allowing for a time step of 2 fs. Non-bonded interactions were truncated at 9 Å, whereas the particle mesh Ewald[70] method was used to account for long-range electrostatic interactions under periodic boundary conditions. Weak harmonic positional restraints with a force constant of 2.0 kcal mol^{-1} $Å^{-2}$ were placed on the complex's non-hydrogen atoms during the minimization and initial equilibration steps. Energy minimization was carried out using the steepest descent algorithm for 500 steps, followed by the conjugate gradient algorithm for another 500 steps. The system was then heated at constant volume to 300 K over 50 ps, followed by equilibration at a constant pressure of 1 atm for another 50 ps. Subsequent unrestrained equilibration (2 ns) and production (50 ns) runs were carried out at a constant temperature of 300 K using a Langevin thermostat[71] with a collision frequency of 2 ps^{-1} and a constant pressure of 1 atm using a Berendsen barostat[72] with a pressure relaxation time of 2 ps.

The protein structures generated by the simulations were clustered using the ART-2 algorithm[73] based on the root-mean-square deviation (RMSD) of the Cα atoms. Cut-off radii of 1.4 and 1.3 Å were used to generate the clusters for the unbound and complex simulations, respectively. The cluster members with the lowest RMSD from their respective centroids were selected as representative structures for structural alignment.

DOI: 10.1021/jacs.6b10234
J. Am. Chem. Soc. 2017, 139, 2245−2256

Computational Alanine Scanning. Computational alanine scanning was carried out on the peptide from 200 equally spaced complex structures extracted from the last 30 ns of the MD simulations deemed stably equilibrated. The differences in the binding free energies ($\Delta\Delta G$) of the wild-type and alanine mutants (or glycine mutant for Ala3) were calculated using the molecular mechanics/generalized Born surface area (MM/GBSA) method.[74] All programs used for MM/GBSA calculations were part of AMBER 11. Molecular mechanical energies were calculated with the sander module of AMBER 11. The polar contribution to the solvation free energy was calculated by the pbsa program using the modified GB model described by Onufriev et al.,[75] and the nonpolar contribution was estimated from the solvent accessible surface area using the linear combinations of pairwise overlaps method[76] with γ set to 0.0072 kcal/Å^2 and β set to zero.[77] The entropy term was not considered due to the high computational cost and the assumption that the entropy of the mutant does not differ considerably from that of the wild type.[78]

Peptide Synthesis and Macrocyclization. The Fmoc-protected azido-functionalized amino acids were synthesized as described previously.[79] All TNKS binding peptides were synthesized manually on Rink Amide MBHA resin (0.65 mmol/g, 100−200 mesh, Novabiochem) using a Vac-Man Laboratory Vacuum Manifold (Promega) according to the standard Fmoc-based solid-phase peptide synthesis (SPPS) method.[80−82] The N-terminus of the peptide was either capped by acetylation or coupled with a spacer aminohexanoic acid followed by 5-carboxytetramethylrhodamine (5-TAMRA). Cell-penetrating peptides were synthesized manually or on an automated microwave peptide synthesizer (Liberty Blue, CEM) on Rink Amide MBHA LL resin (0.38 mmol/g, 100−200 mesh, Novabiochem), and linker m3c was attached to the N-terminal end of the peptides by manual SPPS. All peptides were cleaved from the resin in a TFA cocktail containing 92.5% (v/v) TFA, 2.5% (v/v) water, 2.5% (v/v) triisopropylsilane, and 2.5% (v/v) dichloromethane. The eluate was dried, and the cleaved peptide was precipitated with diethyl ether, redissolved in 1:1 (v/v) water/acetonitrile, filtered, and lyophilized. The crude peptide was purified on a semi-preparative HPLC Agilent 1260 infinity using a Supelcosil ABZ+PLUS column (alkyl-amide phase, 250 mm × 21.2 mm, 5 μm), eluting with a linear gradient system (solvent A: 0.1% (v/v) TFA in water; solvent B: 0.05% (v/v) TFA in acetonitrile). The purity of the peptide was checked on an analytical HPLC (Agilent 1260 Infinity, Supelcosil ABZ+PLUS column (150 mm × 4.6 mm, 3 μm)), eluting with a linear gradient system (solvent A: 0.05% (v/v) TFA in water; solvent B: 0.05% (v/v) TFA in acetonitrile). The purified peptides were lyophilized and analyzed by LCMS.

The double-click reaction was carried out to cross-link the azido-functionalized peptides with dialkynyl functionalized linkers.[83] The aliphatic linkers were purchased from Sigma-Aldrich, and all others were synthesized according to protocols previously described.[56−58] All solvents for the reaction were degassed with nitrogen for 1 h before use. The dialkynyl linker (1.1 equiv) was added to the diazido-peptide in 1:1 (v/v) water and *tert*-butanol under nitrogen before the addition of a solution of copper(II) sulfate pentahydrate (1 equiv), tris(3-hydroxypropyltriazolylmethyl)amine (THPTA, 1 equiv), and sodium ascorbate (3 equiv) in water. The reaction mixture was stirred for 16 h at room temperature and monitored by LCMS. A second aliquot of linker and catalyst was added for those reactions that had not run to completion. The crude product was purified on the semi-preparative HPLC as described above. The purified macrocyclized peptide was lyophilized and analyzed by infrared spectrometry (IR) and high-resolution mass spectrometry.

Protein Purification. Genes for human TNKS1_179−966 and TNKS2_488−649 were purchased from Epoch Life Science, and that for human Axin1_1−80 was purchased from Life Technologies. TNKS1_315−662, TNKS2_488−649, Axin1_1−43, Axin1_1−80 were cloned into expression vector pRSETa (GE Healthcare) or pGEX using standard molecular biology methods. Proteins were expressed and purified according to procedures reported previously with modifications.[53,54] The plasmid containing each construct was transformed to *E. coli* C41(DE3) cells, and the colonies were grown in 2TY media at 37 °C until OD 600 reached 0.6−1.0 and were then induced at 20−25 °C with 0.2−0.5 mM IPTG for 16 h. Cell pellets were collected and resuspended in 50 mM Tris·HCl buffer pH 8.0, 500 mM NaCl, 2 mM DTT, protease inhibitor cocktail (Sigma-Aldrich), 10 mM EDTA for GST-tagged TNKS2_488−649, Axin1_1−43, and Axin1_1−80. For His_6-tagged TNKS1_315−662, 10 mM EDTA was replaced with 10 mM imidazole. The cells were lysed using an Emulsiflex C5 homogenizer, and the lysate was added to either Ni-NTA agarose (QIAGEN) or Glutathione Sepharose 4B beads (GE Healthcare). The bound His_6- or GST-tagged protein was washed with the same resuspension buffer but without the protease inhibitor, and the tag was cleaved with thrombin (25 U per liter of culture) overnight at 25 °C. The desired protein was purified to >95% homogeneity on a size-exclusion gel-filtration column (HiLoad 16/60 Superdex G75) equilibrated with loading buffer of 50 mM HEPES buffer pH 7.5, 300 mM NaCl, 2 mM DTT. For protein crystallization, TNKS2_488−649 was expressed and purified using the same protocol, except that the loading buffer was 20 mM HEPES buffer pH 7.5, 150 mM NaCl, 0.5 mM TCEP.

X-ray Crystallography. For the cocrystal structure of TNKS2 488−649 in complex with cp4n4m5, 0.3 μL of 1 mM TNKS2_488−649 and 5 mM cp4n4m5 in 20 mM HEPES pH 7.5, 150 mM NaCl, 0.5 mM TCEP, 5% (v/v) DMSO were mixed with 0.3 μL of precipitant solution containing 1.60 M trisodium citrate in a sitting drop vapor diffusion experiment at 19 °C. Plate-like crystals grew to their final size in 14 days. For the crystal structure of TNKS2 488−649 in complex with sp4n2m3, a mixture of 0.3 μL of 1 mM TNKS2_488−649 and 2.9 mM cp4n2m3 in 10 mM HEPES pH 7.5, 75 mM NaCl, 0.25 mM TCEP, 5% (v/v) DMSO was mixed with 0.3 μL of precipitant solution containing 3.20 M ammonium sulfate and 0.1 M trisodium citrate pH 5.0 in a sitting drop vapor diffusion experiment at 19 °C. Needle-like crystals appeared after 4 days and grew to the final length of 420 μm after 12 days. Data were collected at Diamond Light Source beamlines I24 and I04-1 and processed with autoPROC[84]/XDS[85] to 1.35 and 1.33 Å, respectively (Table S3). Phases were obtained through molecular replacement using PHASER[86] with PDB 3TWQ[53] as the search model. Iterative model building and refinement were subsequently performed with Coot[87] and REFMAC5.[88] The structures have been deposited in the Protein Data Bank with codes 5BXU (TNKS2 ARC4−cp4n4m5 complex) and 5BXO (TNKS2 ARC4−cp4n2m3 complex). For the comparative analysis, the Cα-atoms of the TNKS2 residues were aligned within a 7 Å radius around the peptide/macrocycle binding site to avoid changes in curvature having a significant impact on the analysis.

Fluorescence Polarization Assays. Fluorescence polarization (FP) assays were performed in 96-well half area black microplates (Corning) on a CLARIOstar microplate reader (BMG labtech) using excitation filter 540−20 nm, dichroic mirror LP 566 nm, and emission filter 590−20 nm. All peptides were dissolved in water as stock solutions. For direct FP assays, the stock concentrations of the TAMRA-labeled peptides were determined based on the 5-TAMRA absorbance at 556 nm (extinction coefficient ε = 89,000 M^{-1} cm^{-1}) measured on a NanoDrop 2000 (Thermo Scientific) and verified by amino acid analysis (Department of Biochemistry, University of Cambridge). TNKS2 ARC4 (488−649) or TNKS1 ARC2−3 (315−662) was diluted 2-fold serially in the assay buffer (50 mM HEPES pH 7.5, 300 mM NaCl, 2 mM DTT, 0.05% (v/v) Tween 20) for a 12-point titration curve in triplicate. The diluted TAMRA-labeled peptide (20 nM, 50 μL) was mixed with the serially diluted TNKS2 ARC4 or TNKS1 ARC2−3 (40−0 μM, 50 μL) in each well and incubated for 30 min at 25 °C before the measurement. Data were analyzed on GraphPad Prism 5.0, and the dissociation constant, K_d, was determined using the following equation assuming the ratio between the concentration of the bound and that of the total TAMRA-labeled peptide is proportional to the fluorescence polarization

$$FP = B + (T - B) * \frac{[(L_0 + P_0 + K_d) - \sqrt{(L_0 + P_0 + K_d)^2 - 4L_0P_0}]}{2L_0}$$

DOI: 10.1021/jacs.6b10234
J. Am. Chem. Soc. 2017, 139, 2245−2256

where *FP* is the fluorescence polarization, *B* is the minimum *FP*, *T* is the maximum *FP*, L_0 is the total concentration of TAMRA-labeled peptide, P_0 is the total concentration of protein, and K_d is the dissociation constant.

For the competition FP assays, the stock concentrations of the unlabeled macrocyclized peptides or the Axin1 fragments were determined by amino acid analysis. TAMRA-labeled pep1 (20 nM) and TNKS2 ARC4 (3 μM) or TNKS1 ARC2−3 (1.2 μM) were incubated in PBS buffer containing 0.05% (v/v) Tween 20. The unlabeled peptide or Axin1 fragment was diluted 2-fold serially in PBS buffer containing 0.05 (v/v) Tween 20 for a 12-point titration curve in triplicate. The diluted peptide or Axin1 fragment (50 μL) was mixed with the TAMRA-pep1/TNKS solution (50 μL) in each well and incubated for 30 min at 25 °C before the measurement was taken. Titrations were performed in triplicate. Data were fitted in GraphPad Prism 5.0 using the equations as described previously.[89]

Circular Dichroism (CD) Spectroscopy. CD spectra were recorded on a Chirascan CD spectrometer (Applied Photophysics), fitted with a water bath and using a 1 mm path length cell. Unlabeled peptides (0.1 mM) were prepared in water, and the spectra were recorded at 25 °C. Four separate measurements were made, and the mean molar ellipticity, θ, was then plotted against the wavelength.

Isothermal Titration Calorimetry (ITC). All ITC experiments were performed on a MicroCal iTC200 (GE Healthcare) at 25 °C. TNKS2 ARC4 (488−649), TNKS1 ARC2−3 (315−662), and Axin1 fragments were dialyzed overnight in PBS and 0.5 mM TCEP. Unlabeled peptides were used in the experiments. The peptide was diluted from the stock solution using the same dialysis buffer, and the effect of buffer dilution was accounted for when preparing TNKS samples. TNKS2 ARC4 (160−280 μM) or TNKS1 ARC2−3 (60−150 μM) was titrated into the sample cell containing the peptide (5−15 μM) or Axin1 fragments (8−12 μM) with an initial injection of 0.2 μL over 0.4 s followed by 19 injections of 2 μL over 4 s with a spacing of 60 s, except for TNKS2 ARC4 and Axin1 fragments for which the spacing was 70 s. Control experiments were performed using the same settings as above except that the cell was filled with dialysis buffer. Data were fitted with nonlinear regression using a one-site binding model from Origin 7.0 (MicroCal, Inc.).[90]

Pull-Down Assay. GST-tagged human Axin1_1−80 was incubated with Glutathione Sepharose 4B beads (GE Healthcare) for 1 h at 4 °C. The beads were washed 3 times with wash buffer (50 mM Tris·HCl pH 8.0, 500 mM NaCl, 2 mM DTT). Approximately 80 μg of GST-tagged Axin1_1−80 (10 μL) on beads was incubated with TNKS2 ARC4 (40 μL, 89 μM) or His_6-tagged TNK1 ARC2−3 (50 μL, 100 μM) for 0.5 h at room temperature. The unbound TNKS protein was washed away with wash buffer (150 μL × 2), and the beads were incubated at room temperature for 0.5 h with the serially diluted unlabeled peptide (50 μL, 0−200 μM). The beads were subsequently washed twice (150 μL × 2), boiled with SDS, and loaded on the SDS-PAGE protein gels. After the run, the gels were stained with Coomassie Brilliant Blue and imaged. The intensities of the bands were analyzed using ImageJ, and the standard deviations were calculated from two independent experiments.

Proteolytic Degradation. Endoproteinase AspN (50 ng, New England BioLabs) was added to a mixture of TAMRA-labeled peptide (400 μM), TAMRA (100 μM), and Endoproteinase AspN enzyme buffer (New England BioLabs), and the volume was made up to 50 μL with sterile water. The reaction was incubated with shaking at 550 rpm at 25 °C. At each time point, a 5 μL aliquot was taken and centrifuged at 10,000 rpm at 4 °C, and the supernatant was diluted 4 times with water before being loaded onto an analytical HPLC (Agilent 1260 Infinity, Supelcosil ABZ+PLUS column (150 mm × 4.6 mm, 3 μm)) and eluted with a linear gradient system (solvent A: 0.05% (v/v) TFA in water; solvent B: 0.05% (v/v) TFA in acetonitrile). TAMRA-labeled T-pep1 was run with a linear gradient of 5−95% solvent B over 5 min, and TAMRA-labeled cp4n2m3 was run with 5−40% solvent B over 20 min. The cleavage of the TAMRA-labeled peptide was monitored at 550 nm, and the integral of the peptide peak was measured against that of TAMRA as the internal standard. After 270 min, the remaining sample containing TAMRA-labeled T-cp4n2m3 was submitted to LCMS, and no mass corresponding to the hydrolyzed macrocyclized peptide could be observed. The plot (Figure S10a) is representative of one of the two independent experiments.

Cellular Uptake Assay. U2OS or HEK 293T cells were grown to 100% confluency before being used in all assays. Cells (10^6) were seeded in glass-bottom dishes (35 mm diameter, MatTek Corporation) and grown for 16 h at 37 °C and 5% CO_2 in 1 mL of DMEM (1×) + GlutaMAX-1 (Life Technologies). Cells were then incubated with TAMRA-labeled peptides (10−40 μM) for 4.5 h, followed by a further 0.5 h incubation with Hoechst 33342 nucleic acid stain (5 μg/mL) at 37 °C and 5% CO_2 before being washed with PBS (2 × 1 mL) and replenished with 1 mL of HBSS (1×) (Life Technologies). Confocal images were taken at 37 °C on a Leica TCS SP5 confocal microscope with sequential excitation at 405 and 543 nm, respectively. The gains were adjusted to be the same among all cell samples.

Cell Toxicity Assay. U2OS cells (2×10^5) or HEK 293T cells (2×10^5) were seeded in a 96-well cell culture plate (Corning Costar) and grown for 16 h at 37 °C and 5% CO_2 in 100 μL of DMEM (1×) + GlutaMAX-1 (Life Technologies) containing 10% (v/v) fetal bovine serum and penicillin-streptomycin. Cells were then incubated with the unlabeled peptides (50 and 100 μM) for 5 h at 37 °C and 5% CO_2. A maximum LDH release control was prepared by adding 10× Lysis Solution (10 μL, Promega) to the cells and incubated at 37 °C for 45 min before the measurement. The supernatant (50 μL) from each well was transferred to a clear flat-bottom 96-well microplate, and the assay was performed using a CytoTox 96 Nonradioactive Cytotoxicity Assay (Promega) according to the manufacturer's protocol. The LDH release indicated by the absorbance at 490 nm was measured on a CLARIOstar microplate reader (BMG Labtech). Data were obtained from triplicate samples, and the standard deviations were calculated from two independent experiments.

TOPFLASH Assay. HEK 293T were grown in Dulbecco's Modified Eagles Medium (DMEM) supplemented with 10% fetal calf serum. Wnt pathway activity was induced by treating cells with 20 mM LiCl (or KCl as control) or conditioned media obtained from L-cells expressing Wnt3A for 6 h. Cells were transfected with the Lipofectamine 2000 transfection reagent according to the manufacturer's protocol (Invitrogen).

For TOPFLASH reporter assays, 100 ng of TOPFLASH plasmid and 10 ng of CMV-Renilla plasmid (as internal control) were used to transfect cells in 24-well plates. Transfected cells were allowed to recover for 8 h, and concurrently treated with unlabeled macrocyclized peptides and Wnt3A conditioned media/LiCl for a further 16 h. TOPFLASH assays were performed using the Dual-Luciferase Reporter Assay System (Promega) as previously described.[91] Relative luciferase values were obtained from triplicate samples (from two independent experiments) by dividing the firefly luciferase values (from TOPFLASH) by the Renilla luciferase values (from CMV-renilla), and standard deviations were calculated.

■ ASSOCIATED CONTENT

Supporting Information

The Supporting Information is available free of charge on the ACS Publications website at DOI: 10.1021/jacs.6b10234.

K_d values for unlabeled peptides from competitive FP, K_d values for TAMRA-labeled peptides from direct FP, crystallographic data, comparison of K_d values for Axin constructs and peptides from FP and ITC, CPP sequences and linkers, K_d values for CPP-conjugated peptides, computational alanine scanning, chemical structures of macrocyclized peptides, representative analytical HPLC and MS spectra, IR spectra before and after macrocyclization, confirmation of the macrocyclization, detailed crystal structures of cp4n4m5 and cp4n2m3 in complex with TNKS2 ARC4, structural comparison of TNKS2 ARC4-cp4n4m5 and TNKS2 ARC4-cp4n2m3 complexes, average side chain B-factors

DOI: 10.1021/jacs.6b10234
J. Am. Chem. Soc. 2017, 139, 2245−2256

of cp4n4m5 and cp4n2m3, *in silico* alignments of TNKS2 ARC4 structures, proteolytic degradation, representative ITC traces for the binding of peptides and Axin1 constructs to TNKS proteins, confocal images of the cellular uptake of TAMRA-labeled peptides, and cytotoxicity assay (PDF)

AUTHOR INFORMATION

Corresponding Authors

*spring@ch.cam.ac.uk
*lsi10@cam.ac.uk

ORCID

Laura S. Itzhaki: 0000-0001-6504-2576

Notes

The authors declare no competing financial interest.

ACKNOWLEDGMENTS

The Itzhaki lab acknowledges support from the Medical Research Council (MRC) (Grant G1002329) and an MRC Confidence in Concept grant. L.S.I. acknowledges the support of a Senior Fellowship from the Medical Research Foundation. The Spring lab acknowledges support from the European Research Council under the European Union's Seventh Framework Programme (FP7/2007-2013)/ERC Grant 279337/DOS. In addition, the group's research was supported by grants from the Engineering and Physical Sciences Research Council, Biotechnology and Biological Sciences Research Council, Medical Research Council, Royal Society, and Wellcome Trust. The work in the Hyvonen lab was funded by the Wellcome Trust Strategic Award (090340/Z/09/Z). We also thank Diamond Light Source UK for the provision of beamtime at beamlines I24 and I04-1 and their staff for helpful assistance and the X-ray crystallography facility at the Department of Biochemistry. We thank the Scherman group (Department of Chemistry, University of Cambridge) for use of their automated peptide synthesizer and the PNAC service (Department of Biochemistry, University of Cambridge).

REFERENCES

(1) Cardote, T. A. F.; Ciulli, A. *ChemMedChem* **2016**, *11* (8), 787−794.
(2) Craik, D. J.; Fairlie, D. P.; Liras, S.; Price, D. *Chem. Biol. Drug Des.* **2013**, *81* (1), 136−147.
(3) Cromm, P. M.; Spiegel, J.; Grossmann, T. N. *ACS Chem. Biol.* **2015**, *10*, 1362−1375.
(4) Henchey, L. K.; Jochim, A. L.; Arora, P. S. *Curr. Opin. Chem. Biol.* **2008**, *12* (6), 692−697.
(5) Loughlin, W. A.; Tyndall, J. D. A.; Glenn, M. P.; Fairlie, D. P. *Chem. Rev.* **2004**, *104* (12), 6085−6117.
(6) Blackwell, H. E.; Grubbs, R. H. *Angew. Chem., Int. Ed.* **1998**, *37* (23), 3281−3284.
(7) Schafmeister, C. E.; Po, J.; Verdine, G. L. *J. Am. Chem. Soc.* **2000**, *122* (24), 5891−5892.
(8) Verdine, G. L.; Hilinski, G. J. *Methods Enzymol.* **2012**, *503*, 3−33.
(9) Walensky, L. D.; Bird, G. H. *J. Med. Chem.* **2014**, *57* (15), 6275−6288.
(10) Condon, S. M.; Morize, I.; Darnbrough, S.; Burns, C. J.; Miller, B. E.; Uhl, J.; Burke, K.; Jariwala, N.; Locke, K.; Krolikowski, P. H.; Kumar, N. V.; Labaudiniere, R. F. *J. Am. Chem. Soc.* **2000**, *122* (13), 3007−3014.
(11) Walensky, L. D.; Kung, A. L.; Escher, I.; Malia, T. J.; Barbuto, S.; Wright, R. D.; Wagner, G.; Verdine, G. L.; Korsmeyer, S. J. *Science* **2004**, *305* (5689), 1466−1470.
(12) Shepherd, N. E.; Hoang, H. N.; Desai, V. S.; Letouze, E.; Young, P. R.; Fairlie, D. P. *J. Am. Chem. Soc.* **2006**, *128* (40), 13284−13289.
(13) Bernal, F.; Tyler, A. F.; Korsmeyer, S. J.; Walensky, L. D.; Verdine, G. L. *J. Am. Chem. Soc.* **2007**, *129* (9), 2456−2457.
(14) Moellering, R.; Cornejo, M.; Davis, T.; Del Bianco, C.; Aster, J.; Blacklow, S.; Kung, A.; Gilliland, D.; Verdine, G.; Bradner, J. *Nature* **2009**, *462*, 182−188.
(15) Ingale, S.; Dawson, P. E. *Org. Lett.* **2011**, *13* (11), 2822−2825.
(16) Stewart, M. L.; Fire, E.; Keating, A. E.; Walensky, L. D. *Nat. Chem. Biol.* **2010**, *6* (8), 595−601.
(17) Grossmann, T. N.; Yeh, J. T.-H.; Bowman, B. R.; Chu, Q.; Moellering, R. E.; Verdine, G. L. *Proc. Natl. Acad. Sci. U. S. A.* **2012**, *109* (44), 17942−17947.
(18) Kawamoto, S. A.; Coleska, A.; Ran, X.; Yi, H.; Yang, C. Y.; Wang, S. *J. Med. Chem.* **2012**, *55* (3), 1137−1146.
(19) Glas, A.; Bier, D.; Hahne, G.; Rademacher, C.; Ottmann, C.; Grossmann, T. N. *Angew. Chem., Int. Ed.* **2014**, *53* (9), 2489−2493.
(20) Guharoy, M.; Chakrabarti, P. *Bioinformatics* **2007**, *23* (15), 1909−1918.
(21) Chang, P.; Coughlin, M.; Mitchison, T. J. *Nat. Cell Biol.* **2005**, *7* (11), 1133−1139.
(22) Chang, W.; Dynek, J. N.; Smith, S. *Biochem. J.* **2005**, *391*, 177−184.
(23) Dynek, J. N.; Smith, S. *Science* **2004**, *304*, 97−100.
(24) Cook, B. D.; Dynek, J. N.; Chang, W.; Shostak, G.; Smith, S. *Mol. Cell. Biol.* **2002**, *22* (1), 332−342.
(25) Sbodio, J. I.; Lodish, H. F.; Chi, N.-W. *Biochem. J.* **2002**, *361*, 451−459.
(26) Seimiya, H.; Smith, S. *J. Biol. Chem.* **2002**, *277* (16), 14116−14126.
(27) Smith, S.; de Lange, T. *Curr. Biol.* **2000**, *10* (20), 1299−1302.
(28) Smith, S.; Giriat, I.; Schmitt, A.; de Lange, T. *Science* **1998**, *282*, 1484−1487.
(29) Huang, S.-M. A.; Mishina, Y. M.; Liu, S.; Cheung, A.; Stegmeier, F.; Michaud, G. A.; Charlat, O.; Wiellette, E.; Zhang, Y.; Wiessner, S.; Hild, M.; Shi, X.; Wilson, C. J.; Mickanin, C.; Myer, V.; Fazal, A.; Tomlinson, R.; Serluca, F.; Shao, W.; Cheng, H.; Shultz, M.; Rau, C.; Schirle, M.; Schlegl, J.; Ghidelli, S.; Fawell, S.; Lu, C.; Curtis, D.; Kirschner, M. W.; Lengauer, C.; Finan, P. M.; Tallarico, J. a; Bouwmeester, T.; Porter, J. A.; Bauer, A.; Cong, F. *Nature* **2009**, *461*, 614−620.
(30) Bao, R.; Christova, T.; Song, S.; Angers, S.; Yan, X.; Attisano, L. *PLoS One* **2012**, *7* (11), e48670.
(31) Gao, J.; Zhang, J.; Long, Y.; Tian, Y.; Lu, X. *Pathol. Oncol. Res.* **2011**, *17* (3), 685−690.
(32) McCabe, N.; Cerone, M. A.; Ohishi, T.; Seimiya, H.; Lord, C. J.; Ashworth, A. *Oncogene* **2009**, *28* (11), 1465−1470.
(33) Shervington, A.; Patel, R.; Lu, C.; Cruickshanks, N.; Lea, R.; Roberts, G.; Dawson, T.; Shervington, L. *Brain Res.* **2007**, *1134*, 45−52.
(34) Zhao, F.; Vermeer, B.; Lehmann, U.; Kreipe, H.; Manns, M. P.; Korangy, F.; Greten, T. F. *Immunology* **2009**, *128*, 134−140.
(35) Lupo, B.; Trusolino, L. *Biochim. Biophys. Acta, Rev. Cancer* **2014**, *1846* (1), 201−215.
(36) Tutt, A. N. J.; Lord, C. J.; McCabe, N.; Farmer, H.; Turner, N.; Martin, N. M.; Jackson, S. P.; Smith, G. C. M.; Ashworth, A. *Cold Spring Harbor Symp. Quant. Biol.* **2005**, *70*, 139−148.
(37) Weil, M. K.; Chen, A. *Curr. Probl. Cacner* **2011**, *35* (1), 7−50.
(38) Al-harthi, L. *J. Neuroimmune Pharmacol.* **2012**, *7* (4), 725−730.
(39) Purro, S. A.; Galli, S.; Salinas, P. C. *J. Mol. Cell Biol.* **2014**, *6*, 75−80.
(40) Fancy, S. P. J.; Baranzini, S. E.; Zhao, C.; Yuk, D. I.; Irvine, K. A.; Kaing, S.; Sanai, N.; Franklin, R. J. M.; Rowitch, D. H. *Genes Dev.* **2009**, *23* (13), 1571−1585.
(41) Fancy, S. P. J.; Harrington, E. P.; Yuen, T. J.; Silbereis, J. C.; Baranzini, S. E.; Bruce, C. C.; Otero, J. J.; Huang, E. J.; Franklin, R. J. M.; Rowitch, D. H. *Nat. Neurosci.* **2012**, *14* (8), 1009−1016.

DOI: 10.1021/jacs.6b10234
J. Am. Chem. Soc. 2017, 139, 2245−2256

(42) Chen, Y.; Guan, Y.; Liu, H.; Wu, X.; Yu, L.; Wang, S.; Zhao, C.; Du, H.; Wang, X. *Biochem. Biophys. Res. Commun.* **2012**, *420* (2), 397−403.
(43) Yu, L.; Guan, Y.; Wu, X.; Chen, Y.; Liu, Z.; Du, H.; Wang, X. *Neurochem. Res.* **2013**, *38* (9), 1904−1913.
(44) Yeh, T.-Y. J.; Sbodio, J. I.; Tsun, Z.-Y.; Luo, B.; Chi, N.-W. *Biochem. J.* **2007**, *402* (2), 279−290.
(45) James, R. G.; Davidson, K. C.; Bosch, K. A.; Biechele, T. L.; Robin, N. C.; Taylor, R. J.; Major, M. B.; Camp, N. D.; Fowler, K.; Martins, T. J.; Moon, R. T. *PLoS One* **2012**, *7* (12), 1−10.
(46) Lau, T.; Chan, E.; Callow, M.; Waaler, J.; Boggs, J.; Blake, R. A.; Magnuson, S.; Sambrone, A.; Schutten, M.; Firestein, R.; Machon, O.; Korinek, V.; Choo, E.; Diaz, D.; Merchant, M.; Polakis, P.; Holsworth, D. D.; Krauss, S.; Costa, M. *Cancer Res.* **2013**, *73* (10), 3132−3144.
(47) Johannes, J. W.; Almeida, L.; Barlaam, B.; Boriack-Sjodin, P. A.; Casella, R.; Croft, R. A.; Dishington, A. P.; Gingipalli, L.; Gu, C.; Hawkins, J. L.; Holmes, J. L.; Howard, T.; Huang, J.; Ioannidis, S.; Kazmirski, S.; Lamb, M. L.; McGuire, T. M.; Moore, J. E.; Ogg, D.; Patel, A.; Pike, K. G.; Pontz, T.; Robb, G. R.; Su, N.; Wang, H.; Wu, X.; Zhang, H. J.; Zhang, Y.; Zheng, X.; Wang, T. *ACS Med. Chem. Lett.* **2015**, *6* (3), 254−259.
(48) Mcgonigle, S.; Chen, Z.; Wu, J.; Chang, P.; Kolber, D.; Ackermann, K.; Twine, N. C.; Shie, J.; Tao, J. *Oncotarget* **2015**, *6* (38), 1.
(49) Hassa, P. O.; Hottiger, M. O. *Front. Biosci., Landmark Ed.* **2008**, *13*, 3046−3082.
(50) Rouleau, M.; Patel, A.; Hendzel, M. J.; Kaufmann, S. H.; Poirier, G. G. *Nat. Rev. Cancer* **2010**, *10* (4), 293−301.
(51) Riffell, J. L.; Lord, C. J.; Ashworth, A. *Nat. Rev. Drug Discovery* **2012**, *11*, 923−936.
(52) Mariotti, L.; Templeton, C. M.; Ranes, M.; Paracuellos, P.; Cronin, N.; Beuron, F.; Morris, E.; Guettler, S. *Mol. Cell* **2016**, *63* (3), 498−513.
(53) Guettler, S.; LaRose, J.; Petsalaki, E.; Gish, G.; Scotter, A.; Pawson, T.; Rottapel, R.; Sicheri, F. *Cell* **2011**, *147* (6), 1340−1354.
(54) Morrone, S.; Cheng, Z.; Moon, R. T.; Cong, F.; Xu, W. *Proc. Natl. Acad. Sci. U. S. A.* **2012**, *109* (5), 1500−1505.
(55) Torres, O.; Yüksel, D.; Bernardina, M.; Kumar, K.; Bong, D. *ChemBioChem* **2008**, *9* (11), 1701−1705.
(56) Lau, Y. H.; de Andrade, P.; Quah, S.-T.; Rossmann, M.; Laraia, L.; Sköld, N.; Sum, T. J.; Rowling, P. J. E.; Joseph, T. L.; Verma, C.; Hyvönen, M.; Itzhaki, L. S.; Venkitaraman, A. R.; Brown, C. J.; Lane, D. P.; Spring, D. R. *Chem. Sci.* **2014**, *5* (5), 1804.
(57) Drewe, W. C.; Neidle, S. *Chem. Commun.* **2008**, 5295−5297.
(58) Sonogashira, K. *J. Organomet. Chem.* **2002**, *653*, 46−49.
(59) Lopes, J. L. S.; Miles, A. J.; Whitmore, L.; Wallace, B. A. *Protein Sci.* **2014**, *23* (12), 1765−1772.
(60) Derossi, D.; Joliot, A. H.; Chassaing, G.; Prochiantz, A. *J. Biol. Chem.* **1994**, *269* (14), 10444−10450.
(61) Montrose, K.; Yang, Y.; Sun, X.; Wiles, S.; Krissansen, G. W. *Sci. Rep.* **2013**, *3*, 1661.
(62) Montrose, K.; Yang, Y.; Krissansen, G. W. *Sci. Rep.* **2014**, *4*, 4900.
(63) Jones, S. W.; Christison, R.; Bundell, K.; Voyce, C. J.; Brockbank, S. M. V; Newham, P.; Lindsay, M. a. *Br. J. Pharmacol.* **2005**, *145* (8), 1093−1102.
(64) Wiedmann, M. M.; Tan, Y. S.; Wu, Y.; Aibara, S.; Xu, W.; Sore, H. F.; Verma, C. S.; Itzhaki, L.; Stewart, M.; Brenton, J. D.; Spring, D. R. *Angew. Chem., Int. Ed.* **2017**, *56*, 1−7.
(65) Dolinsky, T. J.; Czodrowski, P.; Li, H.; Nielsen, J. E.; Jensen, J. H.; Klebe, G.; Baker, N. a. *Nucleic Acids Res.* **2007**, *35*, W522−W525.
(66) Jorgensen, W. L.; Chandrasekhar, J.; Madura, J. D.; Impey, R. W.; Klein, M. L. *J. Chem. Phys.* **1983**, *79* (2), 926.
(67) Lindorff-Larsen, K.; Piana, S.; Palmo, K.; Maragakis, P.; Klepeis, J. L.; Dror, R. O.; Shaw, D. E. *Proteins: Struct., Funct., Genet.* **2010**, *78* (8), 1950−1958.
(68) Case, D. A.; Darden, T. A.; Cheatham, T. E.; Simmerling, C. L.; Wang, J.; Duke, R. E.; Luo, R.; Walker, R. C.; Zhang, W.; Merz, K. M.; Roberts, B.; Wang, B.; Hayik, S.; Roitberg, A.; Seabra, G.; Kolossváry, I.; Wong, K. F.; Paesani, F.; Vanicek, J.; Liu, J.; Wu, X.; Brozell, S. R.; Steinbrecher, T.; Gohlke, H.; Cai, Q.; Ye, X.; Wang, J.; Hsieh, M.-J.; Cui, G.; Roe, D. R.; Mathews, D. H.; Seetin, M. G.; Sagui, C.; Babin, V.; Luchko, T.; Gusarov, S.; Kovalenko, A.; Kollman, P. A. *AMBER 11*, 2010.
(69) Ryckaert, J.-P.; Ciccotti, G.; Berendsen, H. J. C. *J. Comput. Phys.* **1977**, *23* (3), 327−341.
(70) Darden, T.; York, D.; Pedersen, L. *J. Chem. Phys.* **1993**, *98* (12), 10089.
(71) Izaguirre, J. a.; Catarello, D. P.; Wozniak, J. M.; Skeel, R. D. *J. Chem. Phys.* **2001**, *114* (5), 2090.
(72) Berendsen, H. J. C.; Postma, J. P. M.; van Gunsteren, W. F.; DiNola, a; Haak, J. R. *J. Chem. Phys.* **1984**, *81* (8), 3684−3690.
(73) Carpenter, G. A.; Grossberg, S. *Appl. Opt.* **1987**, *26* (23), 4919−4930.
(74) Srinivasan, J.; Cheatham, T. E.; Cieplak, P.; Kollman, P. a.; Case, D. a. *J. Am. Chem. Soc.* **1998**, *120* (37), 9401−9409.
(75) Onufriev, A.; Bashford, D.; Case, D. a. *Proteins: Struct., Funct., Genet.* **2004**, *55* (2), 383−394.
(76) Weiser, J. J.; Shenkin, P. S.; Still, W. C. *J. Comput. Chem.* **1999**, *20* (2), 217−230.
(77) Still, W. C.; Tempczyk, A.; Hawley, R. C.; Hendrickson, T. *J. Am. Chem. Soc.* **1990**, *112* (16), 6127−6129.
(78) Massova, I.; Kollman, P. a. *J. Am. Chem. Soc.* **1999**, *121* (36), 8133−8143.
(79) Lau, Y.; Spring, D. *Synlett* **2011**, *2011* (13), 1917−1919.
(80) Han, S.-Y.; Kim, Y.-A. *Tetrahedron* **2004**, *60* (11), 2447−2467.
(81) Kim, Y.-W.; Grossmann, T. N.; Verdine, G. L. *Nat. Protoc.* **2011**, *6* (6), 761−771.
(82) King, D. S.; Fields, C. G.; Fields, G. B. *Int. J. Pept. Protein Res.* **1990**, *36* (16), 255−266.
(83) Lau, Y. H.; Wu, Y.; de Andrade, P.; Galloway, W. R. J. D.; Spring, D. R. *Nat. Protoc.* **2015**, *10* (4), 585−594.
(84) Vonrhein, C.; Flensburg, C.; Keller, P.; Sharff, A.; Smart, O.; Paciorek, W.; Womack, T.; Bricogne, G. *Acta Crystallogr., Sect. D: Biol. Crystallogr.* **2011**, *67* (4), 293−302.
(85) Kabsch, W. *Acta Crystallogr., Sect. D: Biol. Crystallogr.* **2010**, *66* (2), 125−132.
(86) McCoy, A. J.; Grosse-Kunstleve, R. W.; Adams, P. D.; Winn, M. D.; Storoni, L. C.; Read, R. J. *J. Appl. Crystallogr.* **2007**, *40* (4), 658−674.
(87) Emsley, P.; Lohkamp, B.; Scott, W. G.; Cowtan, K. *Acta Crystallogr., Sect. D: Biol. Crystallogr.* **2010**, *66* (4), 486−501.
(88) Murshudov, G. N.; Skubák, P.; Lebedev, A. A.; Pannu, N. S.; Steiner, R. A.; Nicholls, R. A.; Winn, M. D.; Long, F.; Vagin, A. A. *Acta Crystallogr., Sect. D: Biol. Crystallogr.* **2011**, *67* (4), 355−367.
(89) Wang, Z. X. *FEBS Lett.* **1995**, *360* (2), 111−114.
(90) Freyer, M. W.; Lewis, E. A. *Methods Cell Biol.* **2008**, *84* (07), 79−113.
(91) Korinek, V.; Barker, N.; Morin, P. J.; van Wichen, D.; de Weger, R.; Kinzler, K. W.; Vogelstein, B.; Clevers, H. *Science* **1997**, *275*, 1784−1787.

DOI: 10.1021/jacs.6b10234
J. Am. Chem. Soc. 2017, 139, 2245−2256